

Article

A Comparative Density Functional Theory Study of Hydrogen Storage in Cellulose and Chitosan Functionalized by Transition Metals (Ti, Mg, and Nb)

Omar Faye * , Jerzy A. Szpunar and Ubong Eduok 

Department of Mechanical Engineering, College of Engineering, University of Saskatchewan, 57 Campus Drive, Saskatoon, SK S7N 5A9, Canada

* Correspondence: omf071@usask.ca or omsofaye@yahoo.fr

Abstract: The focus of this work is hydrogen storage in pristine cellulose, chitosan, and cellulose. Chitosan doped with magnesium, titanium, and niobium is analyzed using spin unrestricted plane-wave density functional theory implemented in the Dmol³ module. The results of this study demonstrate that hydrogen interaction with pure cellulose and chitosan occurred in the gas phase, with an adsorption energy of $E_b = 0.095$ eV and 0.090 eV for cellulose and chitosan, respectively. Additionally, their chemical stability was determined as $E_b = 4.63$ eV and $E_b = 4.720$ eV for pure cellulose and chitosan, respectively, by evaluating their band gap. Furthermore, the presence of magnesium, titanium, and niobium on cellulose and chitosan implied the transfer of an electron from metal to cellulose and chitosan. Moreover, our calculations predict that cellulose doped with niobium is the most favorable medium where 6H₂ molecules are stored compared with molecules stored in niobium-doped chitosan with $T_{\max} = 818$ K to release all H₂ molecules. Furthermore, our findings showed that titanium-doped cellulose has a storage capacity of five H₂ molecules, compared to a storage capacity of four H₂ molecules in titanium-doped chitosan. However, magnesium-doped cellulose and chitosan have insufficient hydrogen storage capacity, with only two H₂ molecules physisorbed in the gas phase. These results suggest that niobium-doped cellulose and chitosan may play a crucial role in the search for efficient and inexpensive hydrogen storage media.

Keywords: cellulose; chitosan; hydrogen storage; magnesium; titanium; niobium



Citation: Faye, O.; Szpunar, J.A.; Eduok, U. A Comparative Density Functional Theory Study of Hydrogen Storage in Cellulose and Chitosan Functionalized by Transition Metals (Ti, Mg, and Nb). *Materials* **2022**, *15*, 7573. <https://doi.org/10.3390/ma15217573>

Academic Editor: Oksana V. Komova

Received: 6 September 2022

Accepted: 21 October 2022

Published: 28 October 2022

Publisher's Note: MDPI stays neutral with regard to jurisdictional claims in published maps and institutional affiliations.



Copyright: © 2022 by the authors. Licensee MDPI, Basel, Switzerland. This article is an open access article distributed under the terms and conditions of the Creative Commons Attribution (CC BY) license (<https://creativecommons.org/licenses/by/4.0/>).

1. Introduction

The increase in greenhouse gas emissions in the atmosphere accelerates global warming that threatens life on earth [1]. Therefore, a smooth transition from fossil fuels to clean and sustainable fuels is required. Owing to its high energy content per mass (142 KJ/g) compared to petroleum (47 KJ/g), hydrogen is an optimum clean fuel; when used in fuel cells to generate electricity, it produces water [2,3]. However, the use of H₂ in the future clean economy will still face many obstacles and require various problems to be addressed. When generated, hydrogen has to be stored, and finding a safe and efficient hydrogen storage medium is important for the future hydrogen-based economy. Many hydrogen storage methods have been proposed to date. The most well-known method involves storing gas H₂ in high-pressure tanks [4,5]. However, compressing gaseous hydrogen in the pressure range of 70–80 MPa in a tank creates an additional risk of hydrogen-related embrittlement of the tank walls. Hydrogen can also be stored in cryogenic tanks, although this method requires thermal insulation and cooling of hydrogen below the critical temperature of 33 K. Significant energy is required to liquify H₂, coupled with continuous boil-off. Therefore, to find an alternative way of storing hydrogen, the U.S. Department of Energy (DOE) initiated support for the extensive search for the materials for H₂ storage media in 2003. The criteria set by the DOE for materials for onboard hydrogen storage were specified as (i) high storage capability, that is, 5.5 wt% and 40 g/L at ambient temperatures;

(ii) rapid H₂ release and recharge under moderate conditions; and (iii) long recycling life, that is, more than 1000 recharge and discharge cycles [6]. However, reaching a high storage capacity of 5.5 wt% and 40 g/L under ambient conditions, fast H₂ release, and recharge under moderate conditions is a difficult task. Therefore, to address these challenges, the DEO set an ultimate goal of 6.5 wt% and 60 g/L by 2050 [3]. The following additional criteria were set: an operating temperature (°C) in the range of [−40, 60], a minimum and maximum delivery temperature of −40 and 85 °C, respectively, 1500 operational cycles, delivery pressure in the range [5,6] (bar), and an onboard efficiency of 90% [3]. Furthermore, the rate of charging and discharging was specified as 3–5 min, with a minimum cost of USD 266/kg H₂ [3]. Many materials have been examined and tested to date. There are three ways that hydrogen can interact with the material: physisorption, chemisorption, and the quasi-molecular form of Kubas interaction [2]. During physisorption, hydrogen remains in the molecular form and binds weakly on the substrate, with binding energy in the meV range. This weak binding implies that low temperature is sufficient to desorb the H₂. Such behavior is observed in the metal–organic framework [7–15] and in carbon-based materials [16–19]. However, during chemisorption, hydrogen molecules dissociate into atoms, and the atoms diffuse into the substrate and bind chemically with enthalpy energy in the range of 2 to 4 eV [4]. This strong bonding makes hydrogen desorption difficult, and the process takes place only at high temperatures. This type of bonding occurs in light metal hydrides and chemical hydrides [20,21]. During the Kubas interaction, H₂ bonds stretch without breaking. The bonding strength is between that physisorption and chemisorption in the range of [0.1–0.8 eV]. Such bonding occurs in nanostructure materials and functionalized sorbent materials [20]. There are other requirements for material performance, including the hydrogen storage medium. The material should also be non-toxic, environmentally friendly, and widely available. Biopolymers, such as cellulose and chitosan, satisfy such requirements and show potential for hydrogen storage. Cellulose and chitosan are used in wastewater treatment. They are suitable sorbents for heavy metals, dyes, and organic and emerging contaminants [22,23]. Udoetok et al. [24] proposed chitosan/cellulose glutaraldehyde composite materials synthesized with variable morphology and surface properties with varying levels of self-assembly and cross linking. Their study revealed the structural and synergistic effects of the adsorption properties of cellulose–chitosan composites, as well as their potential application for advanced water treatment, nanomedicine, and drug delivery [24]. Cellulose has attracted attention because it is recyclable and abundant. Furthermore, it can also be used for electronic component applications and in energy devices [25,26]. Mokena et al. [27] summarized cellulose applications in sensors, as well as biomedical, wastewater treatment, and packaging industries. Cellulose combined with graphene has a variety energy storage, electronic, biomedical, optical, and catalysis applications [28]. In addition to cellulose, chitosan also can be used in biomedical [29,30], water treatment [31,32], and environmental applications [33]. However, to the best of our knowledge, no study has been conducted on hydrogen storage in cellulose and chitosan functionalized with magnesium, titanium, and niobium. Therefore, highlighting the effectiveness of these composites for hydrogen storage is important in the ongoing search for materials. In the present study, a density functional theory is used to investigate hydrogen storage in pure cellulose and chitosan. The effect of magnesium-, titanium-, and niobium-coated cellulose and chitosan is also tested to evaluate hydrogen storage characteristics.

2. Computational Methods

We performed a first-principles calculation using spin unrestricted plane-wave density functional theory with the self-consistent field method implemented in the Dmol³ module [34,35]. We used generalized gradient approximation (GGA) with Perdew–Burke–Ernzerhof (PBE) [36] to approximate the exchange–correlation effects on electron–electron interactions. The semi-core-pseudopotentials represent the core electrons as a single effective potential [37]. Double-numerical plus polarization (DNP) used as a

basis set, included the vdW interaction (DFT-D), as proposed by Grimme [38]. Energy minimization was achieved with a convergence tolerance energy of 10^{-5} Ha. The atomic positions were relaxed such that the force acting on each atom was less than 0.002 Ha/Å.

3. Results and Discussion

We investigated the interaction between pure cellulose and transition metals (T.M.s), such as titanium (Ti), magnesium (Mg), and niobium (Nb). Similar calculations were performed for chitosan with the same metals. The strength of the interaction was measured using the following equation:

$$E_b = E_{(A)} + E_{(B)} - E_{(AB)} \quad (1)$$

where $E_{(A)}$ is the total energy of transition metals in an isolated cubic cell of lattice ($a = b = c = 25$ Å), $E_{(B)}$ is the ground energy of cellulose or chitosan, and $E_{(AB)}$ is the total energy of cellulose or chitosan doped with the mentioned TMs. The optimized structures of cellulose and chitosan are displayed in Figure 1.

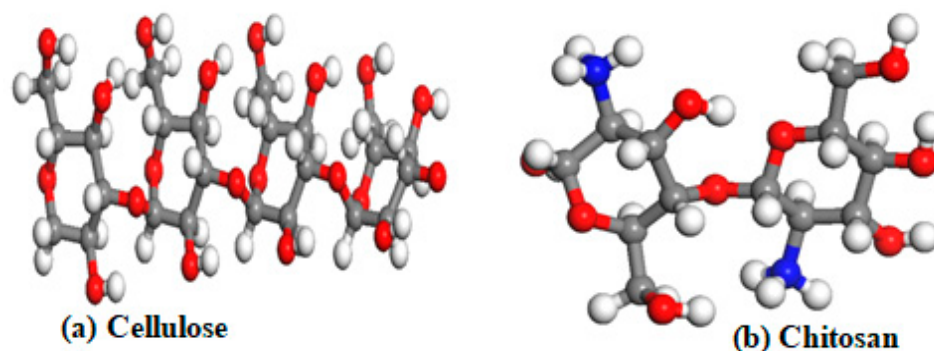


Figure 1. Optimized structures of pure cellulose and pristine chitosan, where red atoms are O, grey atoms are carbon (C), blue atoms are N, and white atoms are H.

We also studied the frontier molecular orbitals to gain insight into the interaction of pristine cellulose and chitosan with additives such as niobium, titanium, and magnesium. Figure 2 depicts the highest occupied molecular orbital (HOMO) (Figure 2A) and the lowest unoccupied molecular orbital (LUMO) (Figure 2B) for pristine cellulose. The same analysis was performed on pristine chitosan, the highest occupied molecular orbital (HOMO) (Figure 2C) and the lowest unoccupied molecular orbital (LUMO) (Figure 2D) or which are also plotted in Figure 2. Furthermore, the energy band gap was determined according to Equation (2).

$$E_g = E_{LUMO} - E_{HOMO} \quad (2)$$

where E_{LUMO} is the energy of the lowest unoccupied molecular orbital (LUMO), and E_{HOMO} is the energy of the highest occupied molecular orbital (HOMO).

The energy difference between HOMO and LUMO orbitals determines the chemical stability of a molecule. These molecular frontiers were calculated using Dmol³ implemented in the material studio.

In Equation (2), a low E_g value indicates the ability to donate electrons to the additive atoms.

Furthermore, the global chemical activity, hardness, and softness parameters were investigated. The ionization energy is defined as $I = -E_{HOMO}$, which is the minimum energy required to remove an electron from a molecule in the gas phase. The electron affinity is defined as $A = -E_{LUMO}$, which is the energy increase that occurs when an electron is added to a molecule in the gas phase. The chemical hardness (α) is $\alpha = (I - A)/2$, measuring the inhibition activity of charge transfer within the molecule. The chemical softness is represented by $S = 1/2\alpha$. In addition, Mulliken electronegativity is defined as $(I + A)/2$, which represents the ability of an atom in a molecule to attract electrons. Finally, the chemical potential and the maximum charge transfer parameter are defined as

$\mu = -(I + A)/2$ and $Dn = (I + A)/2(I - A)$, respectively. These chemical parameters are summarized in Table 1.

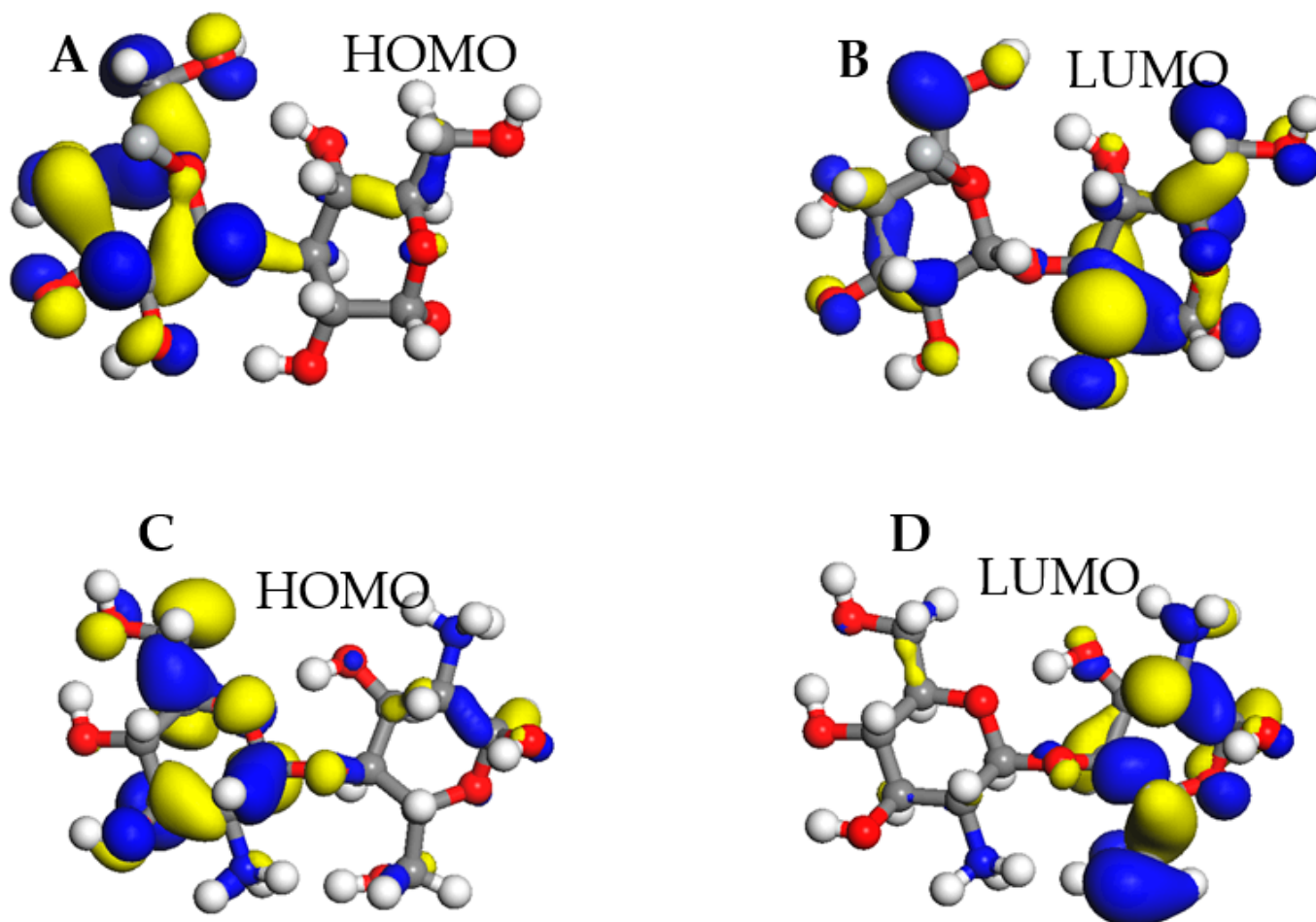
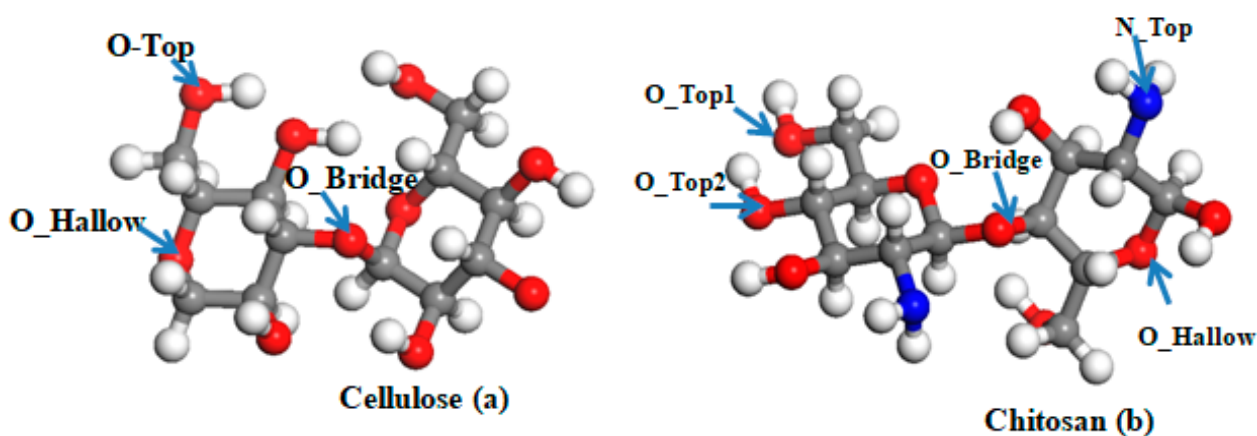


Figure 2. Frontier molecular orbitals, (A,C) stand for HOMO for cellulose and chitosan respectively, and (B,D) stand for LUMO for cellulose and chitosan respectively, the chemical hardness (α), ionization energy (I), electron affinity (A) of pristine cellulose and chitosan.

The HOMO and LUMO energy levels are -16.899 eV and -12.269 eV, respectively, for pristine cellulose compared to -5.918 eV and -1.196 eV for chitosan, as displayed in Table 1. Moreover, the ionization energy, electronegativity, chemical potential, chemical hardness, and chemical softness ranging between -14.584 eV and 16.899 eV for cellulose compared to -3.557 eV to 5.918 eV for chitosan, as shown in Table 1. The maximum charge transfer (Dn) is 3.149 eV and 1.507 eV for cellulose and chitosan, respectively. These results indicate that cellulose and chitosan are highly stable. Because cellulose presents with six carbon asymmetric and three oxygen atoms in a different state, it is important to search for the most favorable adsorption site of magnesium, titanium, and niobium on cellulose. Equation (1) shows that the most favorable site is the oxygen in the bridge position, as shown in Figure 3, with an adsorption energy of 1.890 eV, 3.720 eV, and 3.726 eV for Mg, Ti, and Nb, respectively. A similar investigation was performed on chitosan, with five asymmetric carbons, four oxygens in different states, and one nitrogen type, as shown in Figure 1. The favorable adsorption site of magnesium and titanium is the O_Bridge position, with a binding energy of 1.547 eV and 5.450 eV for Mg and Ti, respectively. However, for the niobium atom, the most favorable site is the N_Top site, as shown in Figure 3, with a binding energy equal to 8.185 eV (Table 2). These high symmetry points are displayed in Figure 3.

Table 1. Chemical parameters of cellulose and chitosan: ionization energy, electron affinity, energy gap, chemical potential, chemical hardness, chemical softness, and maximum charge transfer values.

Cellulose Parameters	
E_{HOMO}	−16.899
E_{LUMO}	−12.269
Ionization energy (I)	16.899
Electron affinity (A)	12.269
Energy gap (Eg)	4.630
Electronegativity (α)	14.584
Chemical potential (μ)	−14.584
Chemical hardness (β)	2.315
Chemical softness (S)	0.216
Maximum charge transfer (Dn)	3.149
Chitosan parameters	
E_{HOMO}	−5.918
E_{LUMO}	−1.196
Ionization energy (I)	5.918
Electron affinity (A)	1.196
Energy gap (Eg)	4.721
Electronegativity (α)	3.557
Chemical potential (μ)	−3.557
Chemical hardness (β)	2.361
Chemical softness (S)	0.212
Maximum charge transfer (Dn)	1.507

**Figure 3.** The adsorption sites (O_Top, O_Hallow, O_Bridge, N_Top, O_Top1, and O_Top2) of cellulose and chitosan.

The calculated enthalpy energy is summarized in Table 2. The interaction of pristine cellulose with titanium is the most stable, with a binding energy of $E_{bTC} = 3.720$ eV and an optimized distance of $d_{CelTi} = 2.340$ Å, followed by interaction between cellulose and niobium, with $E_{bNbCel} = 3.572$ eV and a final distance of $d_{CelNb} = 2.312$ Å. The lowest binding energy is associated with the interaction of cellulose with magnesium, with $E_{bMg} = 1.890$ eV and a minimum distance of $d_{CelMg} = 2.35$ Å. A comparative study was also performed on chitosan, for which the most favorable interaction occurs between

chitosan and niobium, with an adsorption energy of $E_b Nbch = 7.180$ eV and a critical distance of $d_{ChNb} = 2.110$ Å for the nearest atom of chitosan. The enthalpy reaction of titanium with chitosan is $E_b Tich = 5.450$ eV, with a required length of 3.225 Å compared to 3.720 eV in the case of titanium-doped cellulose ($d_{CelTi} = 2.32$ Å). Finally, magnesium adsorption energy on chitosan is 1.547 eV, with an adsorption distance of 3.666 Å compared to 1.890 eV and $d_{CelMg} = 2.544$ Å in the case of magnesium-doped cellulose. Binding energy and bandgap energy were computed using Equations (1) and (2). These results are summarized in Table 2.

Table 2. Equilibrium parameters (binding energy (E_b) and critical distance (d_F (Å))) and the bandgap (E_g (eV)) of the interaction between pristine cellulose and chitosan with magnesium, titanium, and niobium.

Substrate	E_b (eV)	d_F (Å)	E_g (eV)
cellulose + Mg	1.890	2.544	2.46
cellulose + Ti	3.72	2.340	1.50
cellulose + Nb	3.726	2.3	0.25
pristine cellulose			4.630
pristine chitosan			4.720
chitosan + Mg	1.547	3.666	2.770
chitosan + Ti	5.450	3.255	1.570
chitosan + Nb	8.185	2.307	2.980

To investigate the binding process between pure cellulose or chitosan with magnesium, titanium, and niobium, we studied the fluctuation of cellulose's bandgap energy and chitosan's bandgap energy in the presence of the mentioned transition metals. We defined the bandgap of the investigated materials using Equation (2).

The calculated values of the bandgap energy are presented in Table 2. Analysis of the results reveals that the bandgaps of pure cellulose and chitosan are 4.630 and 4.720 eV, respectively, in agreement with results reported in the literature [27,39–41].

When we doped cellulose with magnesium, titanium, and niobium, the energy gap decreased from $E_g = 4.630$ eV to 1.250 eV. The same phenomenon was observed for chitosan coated with Mg, Ti, and Nb, for which the bandgap changed from 4.720 eV pristine chitosan to the lowest value of 1.570 eV. These results suggest that the decrease in the cellulose and chitosan bandgap in the coated system could be related to a charge transfer from the transition metal to the cellulose and chitosan. The same phenomenon was previously observed by Mahmood et al. [42–46]. A similar phenomenon was observed in copper-decorated, nitrogen-doped defective graphene nanoribbons, in which the presence of copper decreased the bandgap from 3.399 eV to 3.352 eV [47].

3.1. Interaction of Hydrogen with Pristine Cellulose and Chitosan

To test the hydrogen storage capacity of cellulose and chitosan, we first investigated the interaction of clean cellulose and chitosan with hydrogen. The strength of the interaction of H_2 with cellulose and chitosan was measured using the following equation:

$$E_{ads} = E_{(S)} + E_{(H_2)} - E_{(S+H_2)} \quad (3)$$

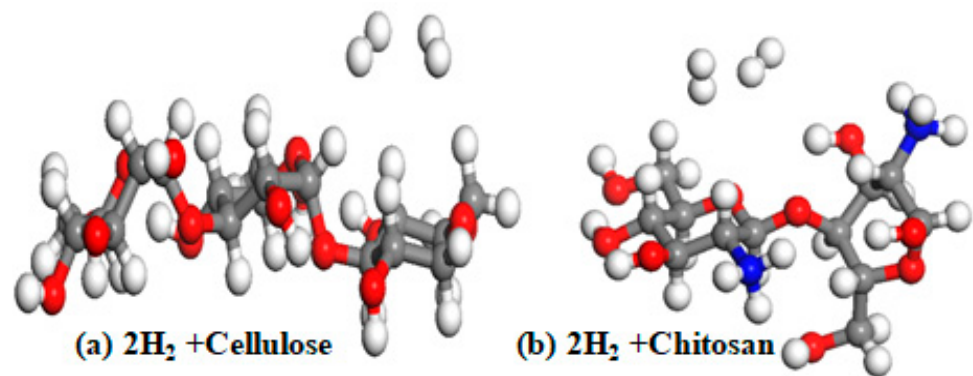
where $E_{(S)}$ is the total energy of the substrate (cellulose or chitosan), $E_{(H_2)}$ is the total energy of isolated hydrogen, and $E_{(S+H_2)}$ is the total interaction energy of cellulose or chitosan with H_2 .

The interaction of hydrogen with cellulose and chitosan was determined using Equation (3); the equilibrium parameters are summarized in Table 3.

Table 3. Enthalpy energy of H₂ with pure cellulose and chitosan.

Cellulose + H ₂	0.095
Cellulose + 2H ₂	0.083
Chitosan + H ₂	0.090
Chitosan + 2H ₂	0.050

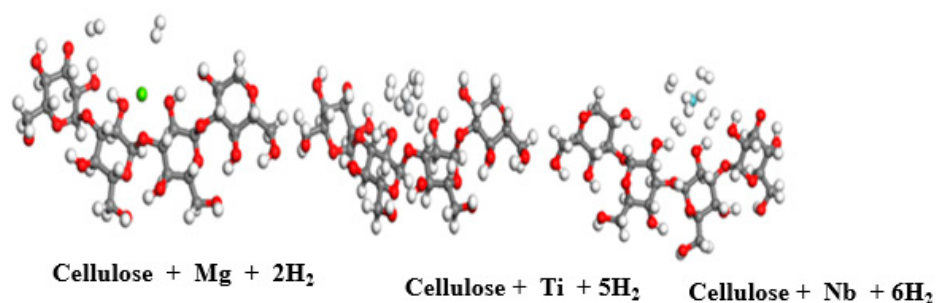
The results presented in Table 2 reveal a weak interaction (physisorption) between hydrogen and cellulose and between H₂ and chitosan. The calculated binding energy between H₂ and cellulose is 0.095 eV, compared to 0.090 eV for chitosan. These results align with results previously reported in the literature [48]. Furthermore, by increasing the number of H₂ molecules in pure cellulose and chitosan to two, a decrease in the binding energy is observed: $E_b = 0.083$ eV and $E_b = 0.050$ eV, for cellulose and chitosan, respectively. The optimized structures are displayed in Figure 4.

**Figure 4.** Optimized pure cellulose structure (a) and pure chitosan structure (b); red atoms are O atom, grey atoms are carbon (C), blue atoms are N, and white atoms are H.

These results show that pure cellulose and pure chitosan are not favorable storage media alone. Therefore, to increase their adsorption capacity, we doped them with magnesium, titanium, and niobium; these results are described in the following section.

3.2. Hydrogen Storage of Cellulose Coated with Magnesium, Niobium, and Titanium

Our hydrogen interaction results with pure cellulose and chitosan show that these new materials are not efficient for hydrogen storage under ambient conditions. Therefore, to enhance the hydrogen storage capacity, we functionalized the materials to increase the active site of hydrogen adsorption. We investigated hydrogen storage on cellulose functionalized with magnesium, niobium, and titanium. The optimized structures are depicted in Figure 5.

**Figure 5.** Optimized structure of magnesium-, titanium-, and niobium-doped cellulose with successive addition hydrogen molecules; red atoms are O, grey atoms are carbon (C), green atoms are Mg, grey metallic atoms are Ti, forest green atoms are Nb, and white atoms are H.

The strength of the binding between hydrogen and cellulose was calculated as follows:

$$E_{ads} = \frac{E_{(Cel+TM_s)} + E_{(nH_2)} - E_{((Cel+TM_s)+nH_2)}}{n} \quad (4)$$

where $E_{(Cel+TM_s)}$ is the total energy of cellulose doped with transition metals (TMs = Mg, Nb, and Ti); $E_{(nH_2)}$ is the total energy of nH_2 molecules; and $E_{((Cel+TM_s)+nH_2)}$ is the total energy of cellulose doped with Mg, Nb, and Ti with $n H_2$ molecules adsorbed on its surface, where n indicates the number of adsorbed H_2 molecules. The adsorption energy was computed using Equation (4); the equilibrium parameters are summarized in Table 4.

Table 4. Equilibrium parameters: binding energy (E_b), critical distance (d_{TM-H} (Å)), distance between hydrogen atoms, and desorption temperature (T_D) between cellulose doped with magnesium, titanium, and niobium.

Number of H ₂ Molecules	E_b (eV)	d_{H-H} (Å)	d_{TM-H} (Å)	T_D (K)
Cell + H ₂ + Nb	0.765	0.896	1.900	978
	0.734	0.897	1.910	938
	0.620	0.870	1.996	792
	0.372	0.840	1.999	475
	0.215	0.831	2.020	274
	0.198	0.789	2.250	253
Cell + Ti + H ₂	0.640	0.850	1.920	818
	0.515	0.858	1.895	658
	0.376	0.831	1.997	480
	0.256	0.807	2.010	327
	0.120	0.792	2.231	153
Cell + Mg + H ₂	0.112	0.758	3.050	143
	0.086	0.757	3.125	109

Cellulose coated with Nb atoms can store six H_2 molecules in the quasi-molecular form with a distance between H atoms in the range of 0.789 to 0.896 Å and a corresponding binding distance in the range of 1.900 to 2.250 Å. Their corresponding adsorption energy fluctuates in the range of 0.198–0.765 eV before reaching saturation, as shown in Table 4. To better visualize the successive adsorption of hydrogen, Figure 6a shows the variation in hydrogen binding energy with niobium-doped cellulose with varying numbers of adsorbed hydrogen molecules. The change in adsorption energy with the number of hydrogen molecules in titanium-doped cellulose is presented in Figure 6b. Figure 6a shows that the binding energy decreases as the number of added H_2 molecules increases. However, in cellulose doped with titanium, the maximum storage capacity is five H_2 molecules in the quasi-molecular form, and the corresponding equilibrium parameters are $d_{H-H} = [0.792 \text{ to } 0.858 \text{ Å}]$ and $d_{TM-H} = [1.895\text{--}2.231 \text{ Å}]$. Furthermore, their corresponding binding energy varies in the range of 0.120 eV to 0.640 eV. Magnesium-doped cellulose is not displayed in Figure 4 because its storage capacity is poor. It can only adsorb two H_2 molecules with the following equilibrium parameters: $d_{H-H} = [0.757\text{--}0.758 \text{ Å}]$, $d_{TM-H} = [3.050\text{--}3.125 \text{ Å}]$, and binding energy in the range of 0.086–0.112 eV, as shown in Table 3. These results for cellulose are in agreement with previously reported results reported in the literature [49].

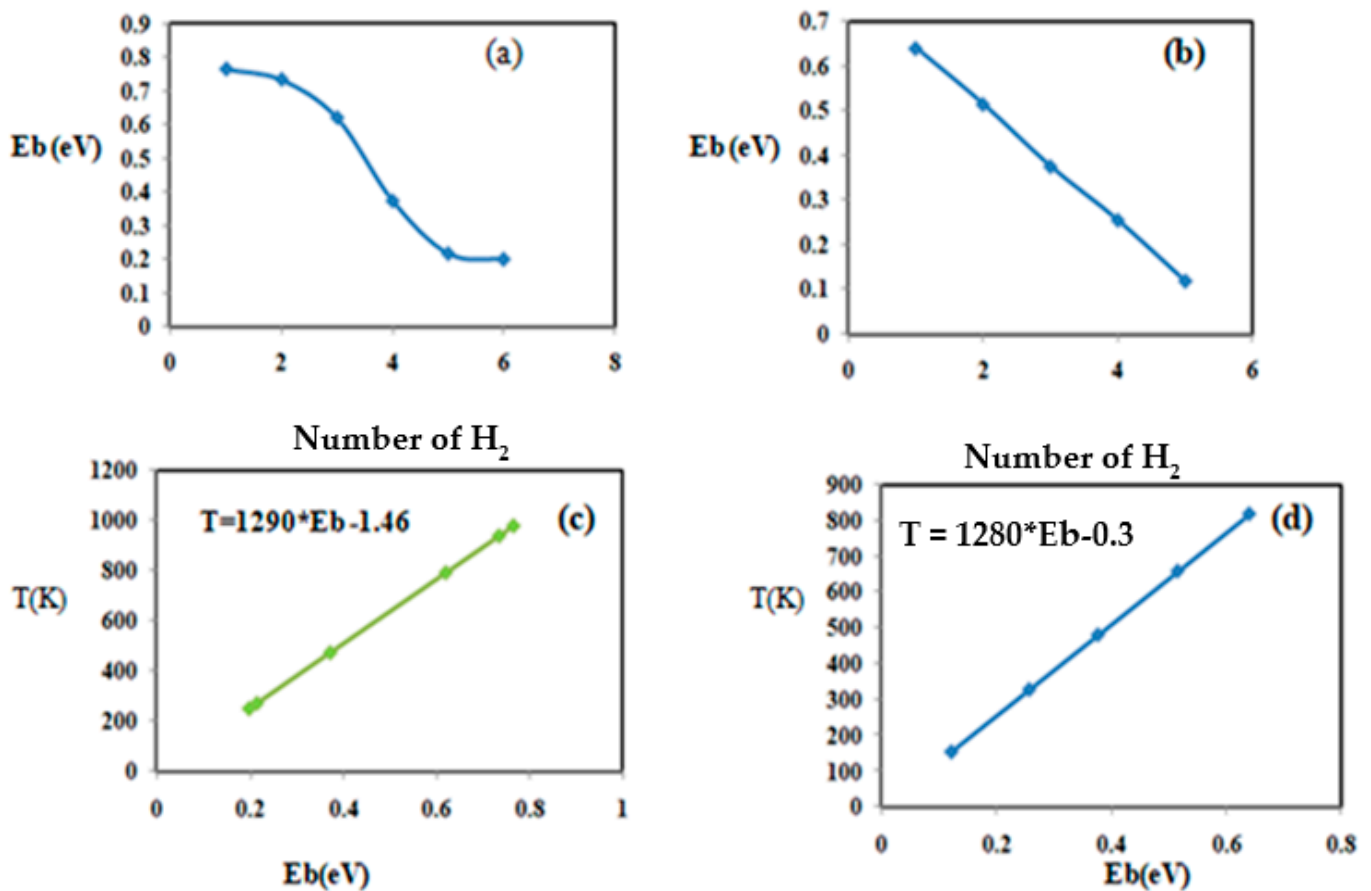


Figure 6. Physical and chemical parameters of the successive addition of H_2 on cellulose. Case (a) represents the variation in the binding energy with respect to the number of hydrogen molecules (cellulose + Nb), case (b) represents the variation in the binding energy with respect to the number of H_2 molecules (cellulose + Ti), case (c) represents the variation in the desorption temperature with respect to the adsorption energy (cellulose + Nb), and case (d) represents the variation in the desorption temperature with respect the adsorption energy of H_2 (cellulose + Ti).

To study the desorption process, we used the van't Hoff equation [2,48,49], as expressed below, to evaluate the desorption temperature (T_D):

$$T_D = \left(\frac{E_{ads}}{K_B} \right) \left(\left(\frac{\Delta S}{R} - \ln \left(\frac{P}{P_0} \right) \right) \right)^{-1} \quad (5)$$

where E_{ads} is the binding energy, K_B represents Boltzmann's constant (8.61733×10^{-5} eV/K), P denotes the pressure (reference pressure $P_0 = 1$ atm), R is the universal gas constant (8.314 JK $^{-1}$ mol $^{-1}$), and ΔS is the entropy change as H_2 moves from the gas to the liquid phase. Assume that $P = 1$ is the atmospheric pressure, and $\Delta S = 130.7$ JK $^{-1}$ mol $^{-1}$ [49,50].

The variation in the binding energy with respect to absorbed H_2 in cellulose-doped titanium is displayed in Figure 6c.

We determine the desorption temperature for the successive addition of H_2 on cellulose doped with niobium, titanium, and magnesium using Equation (5); the results are summarized in Table 4. Cellulose-doped niobium and titanium are the most favorable for hydrogen storage, as shown in Table 4. Therefore, to better understand the correlation between the desorption temperature (T_D) and the adsorption energy, Figure 6c,d shows the desorption temperature as a function of the binding energy for the two most favorable composites (cellulose doped with niobium and cellulose doped with titanium). Figure 6c,d shows a linear relationship between the desorption temperature and the binding energy. The

temperature variation in titanium-doped cellulose is expressed as by $T_D = 1277 \times E_b + 0.55$. In niobium-doped cellulose, the temperature varies: $T_D = 1277 \times E_b - 0.071$. The desorption temperature of the successive hydrogen addition in niobium-doped cellulose is in the interval of 253–978 K, where the maximum temperature is ($T_D = 978$ K) to release all the adsorbed hydrogen at a atmospheric pressure of 1. However, in the case of titanium-doped cellulose, the desorption temperature is within the range of 153–818 K, where $T_D = 818$ K is the maximum temperature required to release all the adsorbed hydrogen at the standard pressure.

3.3. Hydrogen Storage on Chitosan Coated with Magnesium, Niobium, and Titanium

A comparative study was also performed on chitosan doped with magnesium, niobium, and titanium as a hydrogen storage medium. The optimized structure of the chitosan doped with magnesium, titanium, and niobium with the maximum H₂ storage capacity is shown in Figure 7. The first H₂ molecule dissociation is noticeable in titanium- and niobium-doped chitosan, with a binding energy of 0.615 eV for niobium-doped chitosan (Ch_Nb) and 0.405 eV for titanium-doped chitosan (Ch_Ti). However, in magnesium-doped chitosan (Ch_Mg), the first Ch_Mg adsorption energy is 0.142 eV.

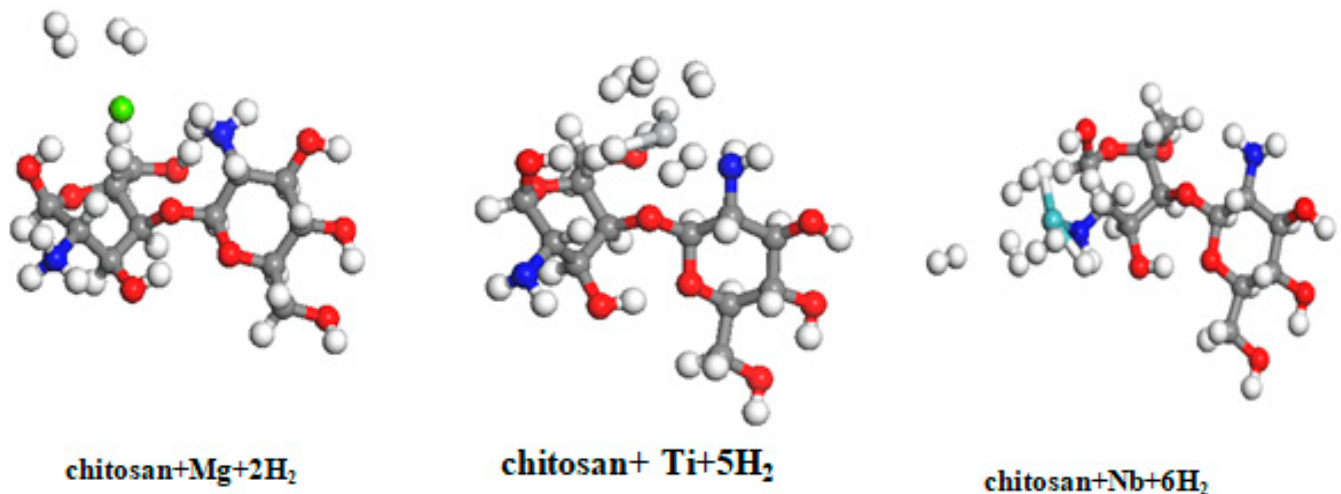


Figure 7. Optimized structure of the interaction of magnesium-, titanium-, and niobium-doped chitosan with the successive addition of hydrogen molecules; red atoms are O, blue atoms are N, grey atoms are carbon (C), green atoms are Mg, grey metallic atoms are Ti, forest green atoms are Nb, and white atoms are H.

The successive adsorption energy of hydrogen with chitosan functionalized with the metals was determined using Equation (3). The calculation results for the subsequent H₂ additions are summarized in Table 5.

Table 5. Successive hydrogen adsorption on chitosan coated with magnesium, titanium, and niobium, along with their corresponding binding distance (d_{H-M}), the distance between hydrogen atoms (d_{H-H}), and the desorption temperature (T_D).

Number of H ₂ Molecules	Binding Energy	d _{H-H} (Å)	d _{H-M} (Å)	T_D (K)
Ch + Mg + H ₂	0.142	0.752	3.141	99
	0.078	0.761	3.304	181
	0.101	0.756	3.280	129
Ch + Ti + H ₂	0.405	0.794	2.025	517

Table 5. Cont.

Number of H ₂ Molecules	Binding Energy	d _{H-H} (Å)	d _{H-M} (Å)	T _D (K)
2H ₂	0.225	0.790	2.068	287
	0.132	0.799	2.011	168
	0.099	0.787	2.076	126
Ch + Nb + H ₂	0.615	0.816	2.012	786
	0.525	0.825	1.995	671
	0.341	0.823	2.020	436
	0.280	0.835	2.045	358
	0.107	0.800	2.890	136

Table 5 shows that H₂ interacted with magnesium-coated chitosan in the gas phase, with an adsorption energy of 0.142 eV for the first adsorbed H₂ molecule, decreasing to 0.078 eV for the second H₂ molecule. In the case of magnesium-coated cellulose, the first adsorption energy of the first H₂ molecule is $E_b = 0.112$ eV and 0.086 eV for the second adsorption. Moreover, the corresponding equilibrium parameters of chitosan are as follow: critical distance (d_{H-Mg}): 3.141 Å for the first H₂ molecule and 3.304 Å for the last added H₂ molecule. The results can be compared to the equilibrium parameters for magnesium-doped cellulose, where d_{H-Mg} = 3.050 Å for the first adsorption and d_{H-Mg} = 3.125 Å for the second adsorption. The desorption temperature (T_D) for these two successive adsorptions is T_D = 181 K and T_D = 99 K, respectively, compared with T_D = 143 K and T_D = 109 K in magnesium-doped cellulose.

To better observe the correlation between the adsorption energy and the number of added H₂ molecules. The maximum hydrogen storage capacity for niobium-coated chitosan is five hydrogen molecules, as shown in Figure 8, and the addition of the six H₂ molecules is not stable. This result indicates that niobium-doped chitosan can store five H₂ molecules in the quasi-molecular form before reaching saturation. Figure 8a,c shows the binding energy for the successive H₂ additions. The desorption temperature (T_D) of successive H₂ adsorption varies in the energy interval of 136–786 K. However, in the case of titanium-doped chitosan, the maximum storage capacity is three H₂ molecules in the quasi-molecular form, with binding energy in the range of 0.132–0.405 eV. A fourth H₂ molecule is in an unstable configuration, with an adsorption energy of 0.099 eV. The corresponding desorption temperature for the successive addition of molecules varies in the range of 168–517 K. To better understand the correlation between the adsorption energy and the corresponding desorption temperature, Figure 8c shows the desorption temperature changes (T_D) with respect to the hydrogen binding energy for niobium-doped chitosan. Figure 8d also displays the desorption temperature (T_D) for different hydrogen adsorption energy for titanium-doped chitosan. Furthermore, the relation between the desorption temperature (T_D) and the binding energy (E_b) is expressed by $T_D = 1290 \times E_b - 1.46$ in niobium-doped chitosan and $T_D = 1280 \times E_b - 0.3$ in the case of titanium-doped chitosan.

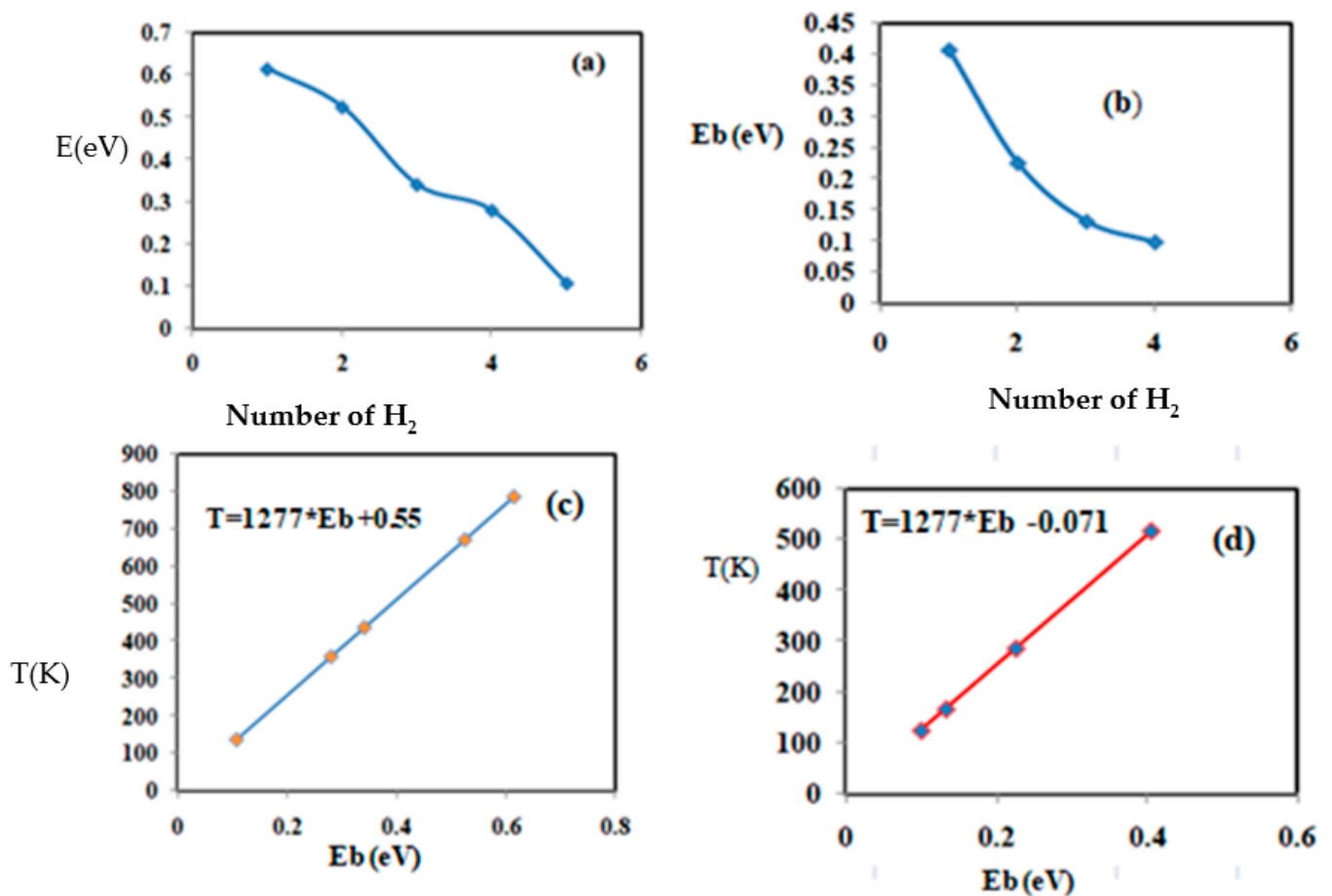


Figure 8. Physical and chemical parameters of the successive addition of H₂ to chitosan. Case (a) represents the variation in the binding energy with respect to the number of hydrogen molecules (chitosan + Nb), case (b) represents the variation in the binding energy with respect to the number of H₂ molecules (chitosan + Ti), case (c) represents the variation in the desorption temperature with respect to the adsorption energy (chitosan + Nb), and case (d) represents the variation in the desorption temperature with respect to the adsorption energy of H₂ (chitosan + Ti).

4. Conclusions

In summary, the present study of hydrogen storage in pure cellulose and chitosan, as well as cellulose and chitosan doped with magnesium, titanium, and niobium using density functional theory highlights the mechanism of hydrogen storage. The results of this investigation show that the interaction between hydrogen and pure cellulose and chitosan takes place in the gas phase (physisorption). Additionally cellulose and chitosan coated with magnesium, titanium, and niobium show exciting results. Our calculations predict that cellulose doped with niobium is the most favorable medium, with a storage capacity of six H₂ molecules, adsorption energy in the range of 0.198–0.765 eV, with system release of all the hydrogen at 978 K. Niobium-doped chitosan can accommodate five H₂ molecules, with binding energy in the range of 0.107–0.615 eV, whereas titanium-doped cellulose has a storage capacity of four H₂ molecules, with binding energy in the range of 0.120–0.640 eV and a maximum desorption temperature of $T_{\max} = 818$ K, compared to a storage capacity of four H₂ molecules in the case of titanium-doped chitosan, with an adsorption range of 0.099–0.405 eV and a maximum desorption temperature of $T_{\max} = 517$ K. However, magnesium-doped cellulose and chitosan show an insufficient hydrogen storage capacity of two H₂ molecules physisorbed. These results demonstrate that niobium-doped cellulose and chitosan might play an important role in the search for efficient and inexpensive hydrogen storage media.

Author Contributions: Conceptualization, investigation and formal analysis, O.F.; writing—review & editing, research methodology, U.E.; Supervision, project administration, funding acquisition, J.A.S. All authors have read and agreed to the published version of the manuscript.

Funding: This work was supported by the National Engineering Research Council of Canada and the Canada Research Chairs program.

Institutional Review Board Statement: Not applicable.

Informed Consent Statement: Not applicable.

Data Availability Statement: Not applicable.

Acknowledgments: We acknowledge access to high-performance supercomputers, Compute Canada, and Plato at the University of Saskatchewan.

Conflicts of Interest: The authors declare no conflict of interest.

References

1. Faye, O.; Eduok, U.; Szpunar, J.A.; Beye, A.C. Two-dimensional carbon nitride (C₃N) nanosheets as promising materials for H₂S and NH₃ elimination: A computational approach. *Phys. E Low-Dimens. Syst. Nanostructures* **2020**, *117*, 113794. [[CrossRef](#)]
2. Faye, O.; Szpunar, J.A. An Efficient Way To Suppress the Competition between Adsorption of H₂ and Desorption of nH₂-Nb Complex from Graphene Sheet: A Promising Approach to H₂ Storage. *J. Phys. Chem. C* **2018**, *122*, 28506–28517. [[CrossRef](#)]
3. Cousins, K.; Zhang, R. Highly Porous Organic Polymers for Hydrogen Fuel Storage. *Polymers* **2019**, *11*, 690. [[CrossRef](#)] [[PubMed](#)]
4. Jena, P. Materials for Hydrogen Storage: Past, Present, and Future. *J. Phys. Chem. Lett.* **2011**, *2*, 206–211. [[CrossRef](#)]
5. Von Colbe, J.B.; Ares, J.-R.; Barale, J.; Baricco, M.; Buckley, C.; Capurso, G.; Gallandat, N.; Grant, D.M.; Guzik, M.N.; Jacob, I.; et al. Application of hydrides in hydrogen storage and compression: Achievements, outlook and perspectives. *Int. J. Hydrogen Energy* **2019**, *44*, 7780–7808. [[CrossRef](#)]
6. Satyapal, S.; Petrovic, J.; Read, C.; Thomas, G.; Ordaz, G. The U.S. Department of Energy's National Hydrogen Storage Project: Progress towards meeting hydrogen-powered vehicle requirements. *Catal. Today* **2007**, *120*, 246–256. [[CrossRef](#)]
7. Gao, Y.; Wu, X.; Zeng, X.C. Designs of fullerene-based frameworks for hydrogen storage. *J. Mater. Chem. A* **2014**, *2*, 5910–5914. [[CrossRef](#)]
8. Ren, J.; Musyoka, N.M.; Langmi, H.W.; North, B.C.; Mathe, M.; Kang, X.; Liao, S. Hydrogen storage in Zr-fumarate MOF. *Int. J. Hydrogen Energy* **2015**, *40*, 10542–10546. [[CrossRef](#)]
9. Mahmood, A.; Khan, S.U.-D.; Rana, U.A.; Tahir, M.H. Red shifting of absorption maxima of phenothiazine based dyes by incorporating electron-deficient thiadiazole derivatives as π -spacer. *Arab. J. Chem.* **2019**, *12*, 1447–1453. [[CrossRef](#)]
10. Mahmood, A.; Hussain Tahir, M.; Irfan, A.; Khalid, B.; Al-Sehemi, A.G. Computational Designing of Triphenylamine Dyes with Broad and Red-shifted Absorption Spectra for Dye-sensitized Solar Cells using Multi-Thiophene Rings in π -Spacer. *Bull. Korean Chem. Soc.* **2015**, *36*, 2615–2620. [[CrossRef](#)]
11. Mahmood, A.; Irfan, A. Effect of fluorination on exciton binding energy and electronic coupling in small molecule acceptors for organic solar cells. *Comput. Theor. Chem.* **2020**, *1179*, 112797. [[CrossRef](#)]
12. Mahmood, A.; Irfan, A.; Ahmad, F.; Janjua, M.R.S.A. Quantum chemical analysis and molecular dynamics simulations to study the impact of electron-deficient substituents on electronic behavior of small molecule acceptors. *Comput. Theor. Chem.* **2021**, *1204*, 113387. [[CrossRef](#)]
13. Mahmood, A.; Khan, S.U.-D.; Rana, U.A.; Janjua, M.R.S.A.; Tahir, M.H.; Nazar, M.F.; Song, Y. Effect of thiophene rings on UV/visible spectra and non-linear optical (NLO) properties of triphenylamine based dyes: A quantum chemical perspective. *J. Phys. Org. Chem.* **2015**, *28*, 418–422. [[CrossRef](#)]
14. Wei, T.; Lim, K.; Tseng, Y.; Chan, S. A review on the characterization of hydrogen in hydrogen storage materials. *Renew. Sustain. Energy Rev.* **2017**, *79*, 1122–1133. [[CrossRef](#)]
15. Ozturk, Z.; Baykasoglu, C.; Celebi, A.T.; Kirca, M.; Mugan, A.; To, A.C. Hydrogen storage in heat welded random CNT network structures. *Int. J. Hydrogen Energy* **2015**, *40*, 403–411. [[CrossRef](#)]
16. Manilov, A.; Skryshevsky, V. Hydrogen in porous silicon—A review. *Mater. Sci. Eng. B* **2013**, *178*, 942–955. [[CrossRef](#)]
17. Faye, O.; Hussain, T.; Kartan, A.; Szpunar, J.A. Tailoring the capability of carbon nitride (C₃N) nanosheets toward hydrogen storage upon light transition metal decoration. *Nanotechnology* **2019**, *30*, 075404. [[CrossRef](#)]
18. Kato, R.; Nishide, H. Polymers for carrying and storing hydrogen. *Polym. J.* **2018**, *50*, 77–82. [[CrossRef](#)]
19. Xiong, R.; Sang, G.; Zhang, G.; Yan, X.; Li, P.; Yao, Y.; Luo, D.; Chen, C.; Tang, T. Evolution of the active species and catalytic mechanism of Ti doped NaAlH₄ for hydrogen storage. *Int. J. Hydrogen Energy* **2017**, *42*, 6088–6095. [[CrossRef](#)]
20. Aizat, M.A.; Aziz, F. Chitosan nanocomposite application in wastewater treatments. In *Nanotechnology in Water and Wastewater Treatment*; Elsevier: Amsterdam, The Netherlands, 2019; pp. 243–265. [[CrossRef](#)]
21. Abou-Zeid, R.E.; Khiari, R.; El-Wakil, N.; Dufresne, A. Current State and New Trends in the Use of Cellulose Nanomaterials for Wastewater Treatment. *Biomacromolecules* **2019**, *20*, 573–597. [[CrossRef](#)]

22. Udoetok, I.A.; Wilson, L.D.; Headley, J.V. Self-Assembled and Cross-Linked Animal and Plant-Based Polysaccharides: Chitosan–Cellulose Composites and Their Anion Uptake Properties. *ACS Appl. Mater. Interfaces* **2016**, *8*, 33197–33209. [[CrossRef](#)] [[PubMed](#)]
23. Dutta, S.; Kim, J.; Ide, Y.; Kim, J.H.; Hossain, M.S.A.; Bando, Y.; Yamauchi, Y.; Wu, K.C.-W. 3D network of cellulose-based energy storage devices and related emerging applications. *Mater. Horiz.* **2017**, *4*, 522–545. [[CrossRef](#)]
24. Chen, W.; Yu, H.; Lee, S.-Y.; Wei, T.; Li, J.; Fan, Z. Nanocellulose: A promising nanomaterial for advanced electrochemical energy storage. *Chem. Soc. Rev.* **2018**, *47*, 2837–2872. [[CrossRef](#)]
25. Nainggolan, I.; Shantini, D.; Nasution, T.I.; Derman, M.N. Role of Metals Content in Spinach in Enhancing the Conductivity and Optical Band Gap of Chitosan Films. *Adv. Mater. Sci. Eng.* **2015**, *2015*, 702815. [[CrossRef](#)]
26. Trache, D.; Thakur, V.; Boukherroub, R. Cellulose Nanocrystals/Graphene Hybrids—A Promising New Class of Materials for Advanced Applications. *Nanomaterials* **2020**, *10*, 1523. [[CrossRef](#)]
27. Wang, W.; Meng, Q.; Li, Q.; Liu, J.; Zhou, M.; Jin, Z.; Zhao, K. Chitosan Derivatives and Their Application in Biomedicine. *Int. J. Mol. Sci.* **2020**, *21*, 487. [[CrossRef](#)] [[PubMed](#)]
28. Morin-Crini, N.; Lichtfouse, E.; Torri, G.; Crini, G. Applications of chitosan in food, pharmaceuticals, medicine, cosmetics, agriculture, textiles, pulp and paper, biotechnology, and environmental chemistry. *Environ. Chem. Lett.* **2019**, *17*, 1667–1692. [[CrossRef](#)]
29. Yang, R.; Li, H.; Huang, M.; Yang, H.; Li, A. A review on chitosan-based flocculants and their applications in water treatment. *Water Res.* **2016**, *95*, 59–89. [[CrossRef](#)]
30. Vidal, R.R.L.; Moraes, J.S. Removal of organic pollutants from wastewater using chitosan: A literature review. *Int. J. Environ. Sci. Technol.* **2019**, *16*, 1741–1754. [[CrossRef](#)]
31. Peter, S.; Lyczko, N.; Gopakumar, D.; Maria, H.J.; Nzihou, A.; Thomas, S. Chitin and Chitosan Based Composites for Energy and Environmental Applications: A Review. *Waste Biomass-Valorization* **2020**, *12*, 4777–4804. [[CrossRef](#)]
32. Delley, B. An all-electron numerical method for solving the local density functional for polyatomic molecules. *J. Chem. Phys.* **1990**, *92*, 508–517. [[CrossRef](#)]
33. Delley, B. From molecules to solids with the DMol3 approach. *J. Chem. Phys.* **2000**, *113*, 7756–7764. [[CrossRef](#)]
34. Perdew, J.P.; Burke, K.; Ernzerhof, M. Generalized gradient approximation made simple. *Phys. Rev. Lett.* **1996**, *77*, 3865. [[CrossRef](#)] [[PubMed](#)]
35. Perdew, J.P.; Chevary, J.A.; Vosko, S.H.; Jackson, K.A.; Pederson, M.R.; Singh, D.J.; Fiolhais, C. Erratum: Atoms, molecules, solids, and surfaces: Applications of the generalized gradient approximation for exchange and correlation. *Phys. Rev. B* **1992**, *48*, 4978. [[CrossRef](#)]
36. Fritsch, D.; Koepernik, K.; Richter, M.; Eschrig, H. Transition Metal Dimers as Potential Molecular Magnets. *J. Comput. Chem.* **2008**, *1145*, 2210–2219. [[CrossRef](#)]
37. Simão, C.D.; Reparaz, J.S.; Wagner, M.R.; Graczykowski, B.; Kreuzer, M.; Ruiz-Blanco, Y.B.; García, Y.; Malho, J.-M.; Goñi, A.R.; Ahopelto, J.; et al. Optical and mechanical properties of nanofibrillated cellulose: Toward a robust platform for next-generation green technologies. *Carbohydr. Polym.* **2015**, *126*, 40–46. [[CrossRef](#)]
38. Abd-Elrahman, M.I.; Ahmed, M.O.; Abdel-Aleem, J.A. Optical properties of cellulose derivatives blend film carrying a chalcogenide material. *Mater. Sci. Semicond. Process.* **2013**, *16*, 1052–1056. [[CrossRef](#)]
39. Hai, T.A.P.; Sugimoto, R. Fluorescence control of chitin and chitosan fabricated *via* surface functionalization using direct oxidative polymerization. *RSC Adv.* **2018**, *8*, 7005–7013. [[CrossRef](#)]
40. Mahmood, A. Photovoltaic and Charge Transport Behavior of Diketopyrrolopyrrole Based Compounds with A–D–A–D–A Skeleton. *J. Clust. Sci.* **2019**, *30*, 1123–1130. [[CrossRef](#)]
41. Mahmood, A.; Abdullah, M.I.; Nazar, M.F. Quantum Chemical Designing of Novel Organic Non-Linear Optical Compounds. *Bull. Korean Chem. Soc.* **2014**, *35*, 1391–1396. [[CrossRef](#)]
42. Khalid, M.; Khan, M.U.; Shafiq, I.; Hussain, R.; Ali, A.; Imran, M.; Braga, A.A.C.; Rehman, M.F.U.; Akram, M.S. Structural modulation of π -conjugated linkers in D– π –A dyes based on triphenylamine dicyanovinylene framework to explore the NLO properties. *R. Soc. Open Sci.* **2021**, *8*, 210570. [[CrossRef](#)] [[PubMed](#)]
43. Khalid, M.; Khan, M.U.; Shafiq, I.; Hussain, R.; Mahmood, K.; Hussain, A.; Jawaria, R.; Hussain, A.; Imran, M.; Assiri, M.A.; et al. NLO potential exploration for D– π –A heterocyclic organic compounds by incorporation of various π -linkers and acceptor units. *Arab. J. Chem.* **2021**, *14*, 103295. [[CrossRef](#)]
44. Khalid, M.; Lodhi, H.M.; Khan, M.U.; Imran, M. Structural parameter-modulated nonlinear optical amplitude of acceptor– π –D– π -donor-configured pyrene derivatives: A DFT approach. *RSC Adv.* **2021**, *11*, 14237–14250. [[CrossRef](#)]
45. Singla, M.; Jaggi, N. Enhanced hydrogen sensing properties in copper decorated nitrogen doped defective graphene nanoribbons: DFT study. *Phys. E Low-Dimens. Syst. Nanostructures* **2021**, *131*, 114756. [[CrossRef](#)]
46. Lousada, C.M. Wood cellulose as a hydrogen storage material. *Int. J. Hydrogen Energy* **2020**, *45*, 14907–14914. [[CrossRef](#)]
47. Lee, H.; Choi, W.I.; Ihm, J. Combinatorial Search for Optimal Hydrogen-Storage Nanomaterials Based on Polymers. *Phys. Rev. Lett.* **2006**, *97*, 056104. [[CrossRef](#)]
48. Durgun, E.; Ciraci, S.; Yildirim, T. Functionalization of carbon-based nanostructures with light transition-metal atoms for hydrogen storage. *Phys. Rev. B* **2008**, *77*, 085405. [[CrossRef](#)]

-
49. Alhameedi, K.; Karton, A.; Jayatilaka, D.; Hussain, T. Metal functionalized inorganic nano-sheets as promising materials for clean energy storage. *Appl. Surf. Sci.* **2019**, *471*, 887–892. [[CrossRef](#)]
 50. Züttel, A. Materials for hydrogen storage. *Mater. Today* **2003**, *6*, 24–33. [[CrossRef](#)]